energies

MDPI

Article

Cooling and Mechanical Performance Analysis of a Trapezoidal Thermoelectric Cooler with Variable Cross-Section

Tianbo Lu [1,2], Yuqiang Li [1,*], Jianxin Zhang [1], Pingfan Ning [1] and Pingjuan Niu [1,*]

[1] Engineering Research Center of High Power Solid State Lighting Application System, Ministry of Education, Tiangong University, Tianjin 300387, China; 1720031032@tiangong.edu.cn (T.L.); zhangjianxin@tiangong.edu.cn (J.Z.); ningpingfan@tiangong.edu.cn (P.N.)

[2] School of Mechanical Engineering, Tiangong University, Tianjin 300387, China

* Correspondence: liyuqiang@tiangong.edu.cn (Y.L.); niupingjuan@tiangong.edu.cn (P.N.)

Received: 9 October 2020; Accepted: 17 November 2020; Published: 19 November 2020

Abstract: In this study, a full-scale three-dimensional trapezoidal thermoelectric cooler model is constructed to study its cooling performance and mechanical reliability using finite element simulation. Temperature dependent material properties are considered in this work. The boundary conditions similar to those in a real experimental environment are applied. The effects of the input electrical current and geometry of the thermoelectric leg on the cooling performance and reliability of a trapezoidal thermoelectric cooler are analyzed, and a comparison is made with a rectangular thermoelectric cooler. The results indicate that increasing the leg height and the variable cross-sectional design of the leg can improve the cooling performance of the trapezoidal thermoelectric cooler. Compared to the original rectangular thermoelectric cooler, the minimum chip temperature was reduced by 0.87% under the trapezoidal thermoelectric cooler with optimized geometry. Furthermore, increasing the leg height enhances the mechanical reliability of the trapezoidal thermoelectric cooler, while the trapezoidal design of the leg reduces its mechanical reliability. The maximum von Mises stress of the leg for the trapezoidal thermoelectric cooler with optimal cooling performance increased by 40.1%. The results of this work provide useful guidance for the structural design of trapezoidal thermoelectric coolers.

Keywords: trapezoidal thermoelectric cooler; variable cross-sectional area; cooling performance; thermal stress analysis

1. Introduction

The thermal management of electronic devices has attracted increased attention in recent years. With the power density of the electronic device increases, more heat is generated by electronic devices. Excessive chip temperature will reduce the reliability of the device [1]. Many advanced passive cooling techniques such as heat pipe cooling [2], micro-channel cooling [3], phase change cooling [4] and nanofluid cooling [5,6] have effectively prevented the chip from overheating. Nevertheless, these passive cooling methods cannot quickly remove the high heat fluxes and effectively control the chip temperature. An effective cooling method needs to be developed to solve the thermal management problem of electronic devices.

The thermoelectric cooler (TEC) is an attractive cooling technology, which takes advantage of the Peltier effect to remove the localized heat fluxes of electronic devices and control the chip temperature, reflecting significant advantages in thermal management [7]. A TEC contains a number of thermoelectric legs, which are connected by copper slices and encapsulated by ceramic substrates. The TEC has many advantages over conventional refrigeration equipment including good reliability, no moving mechanical modules, a small dimension, quiet operation and zero pollution [8].

In spite of their advantages, thermoelectric coolers (TECs) are still not widely used in account of their low thermoelectric conversion efficiency and high price. Many attempts have been made to enhance the cooling performance of TECs, and researchers have improved the conversion efficiency in two main ways. The first way involves improving the figure of merit (ZT) by finding new thermoelectric materials and doping in the original thermoelectric material [9,10]. In addition, numerous researchers have strived to optimize the structure of TECs using commercial thermoelectric materials [11].

Some researchers have found that the height and cross-sectional area of the leg have a remarkable influence on the TEC performance. Zhu et al. [12] found that the cooling performance of the TEC is improved and its response time shortened with the ratio of the leg height to the leg cross-sectional area decreased using finite element analysis. Huang et al. [13] selected the number of thermoelectric legs, leg height and fill ratio of the thermoelectric pairs as optimization variables and used a simplified conjugated-gradient algorithm to obtain the maximum cooling capacity of the TEC. Abid et al. [14] altered the height and cross-sectional area of the legs to optimize cooling performance of TECs by simulation and experimental verification. Gong et al. [15] found a smaller leg height and larger cross-sectional area of the leg are conducive to enhancing cooling performance and reliability of rectangular TECs.

Nevertheless, it should be noted that commercial thermoelectric legs are limited to rectangular shape with a constant cross-sectional area. This is mainly because the shape of the legs is limited by traditional processing techniques. Recently, with the rapid development of additive manufacturing technology, the limitations of traditional manufacturing processes have been overcome, enabling the manufacture of thermoelectric legs with complex shapes [16–18]. Consequently, it is of great significance to study the effect of differently shaped legs on the thermoelectric performance and reliability of thermoelectric devices. Many researchers have studied some new shapes of thermoelectric legs with non-constant cross-sectional areas, such as trapezoidal-shaped [19,20], X-shaped [21] and Y-shaped legs [22]. Considering the simplicity of the manufacturing process, the trapezoidal-shaped leg structure has been gradually studied using analytical methods or finite element methods. In spite of a number of studies having focused on the influence of a trapezoidal-shaped leg on the thermoelectric performance of thermoelectric device, they are basically related to the thermoelectric generator. Since the leg structure of variable cross-sectional areas affects the thermal resistance and electrical resistance of legs, the performance evaluation of TECs with non-constant cross-sectional areas is an important research issue, and few studies have focused on the influence of trapezoidal-shaped leg structure on TEC performance. Lin et al. [23] introduced trapezoid-type two-stage p-n pairs in a two-stage TEC. They proved that this structure can enhance performance compared with the traditional rectangular-shaped leg structure. Lv et al. [24] studied the effect of the single-stage TEC with no-constant cross-sectional area on transient supercooling performance by comparing it with a TEC with constant cross-sectional area. Gao et al. [25] designed the new two-stage TEC with non-constant cross-sectional areas. They adjusted cross-sectional area ratios of the hot side to the cold side of different stages to enhance transient supercooling performance. Qiu et al. [26] analyzed the influences of the leg shape, connection layer thickness and temperature difference between hot and cold ends on the performance of a TEC with a variable cross-sectional area using numerical and mathematical models. Lamba et al. [27] made use of an optimization algorithm to find optimal values of design variables for optimizing the performance of a single-stage trapezoidal TEC, and studied the effect of the Thomson effect on the cooling capacity of the TEC.

When designing thermoelectric devices, it is of importance to enhance their thermoelectric performance. In addition, reliability should be taken into account. The failure of thermoelectric devices is mainly due to the mismatched thermal expansion coefficients of different components. Various defects are caused by thermal stress, which reduce the lifespan of thermoelectric devices, causing their eventual failure [28]. Hence, it is necessary to research the thermal stress distribution of thermoelectric devices and find high stress locations within them. These data are helpful to improve the reliability and lifespan of the devices, and many researchers have thus conducted work on thermal stress in

the last few years [29–31]. Many of them have analyzed the thermal stress of thermoelectric devices with variable cross-sectional areas. Merbati et al. [32] studied the thermal stress distribution of the trapezoidal thermoelectric device, and found that trapezoidal-shaped legs could decrease the maximum thermal stress within thermoelectric generator. Erturun et al. [33] analyzed the effects of various leg shapes on the thermo-mechanical performance of thermoelectric generators. Yilbas et al. [34] studied a horizontal and variable cross-sectional thermoelectric generator, and showed that the tapered legs can decrease thermal stress compared with the rectangular-shaped legs. Ibeagwu et al. [35] clarified the influence of various leg configurations on thermal stress. They showed that optimization of leg shape is an effective method to reduce thermal stress. Most articles focus on research of thermal stress in thermoelectric generators due to the fact that thermoelectric generators operate in environments with large temperature differences between the hot side and cold side. Thermal stress is, therefore, much more likely to occur. The temperature difference between the hot side and cold side generated by the TEC is relatively small compared with that of a thermoelectric generator. In fact, when a large electrical current is applied, a TEC generates a great deal of heat inside the device due to the Joule heating effect. The thermo-mechanical characteristics of TECs are thus affected. Therefore, it is of importance to investigate the thermal stress distribution of TECs for improving their reliability. However, there are few articles that have studied the thermal stress of TECs at present. Wang et al. [36] investigated the thermal deformation of a TEC and explained its cause through experiments. Gong et al. [37] studied the effects of the electrical current, leg height, thickness of substrates and contact layers on the thermal stress of a TEC. Gong et al. [38] studied the transient thermal stress gradient of a TEC when a variable load was applied to its cold surface.

These articles show the importance of analyzing the performance and thermal stress of trapezoidal TECs. However, most of these studies use thermal resistance models to analyze the performance of trapezoidal TECs. The Joule heating effect and Thomson effect are assumed to be symmetrically distributed in the thermoelectric leg in these studies. The local thermal resistance and electrical conductance of the trapezoidal-shaped leg vary with different cross-sectional areas of the legs along the leg height. Therefore, it is not appropriate to assume that the symmetrical distribution of both effects in the trapezoidal TEC. Moreover, to the best of our knowledge, at present no studies have systematically researched the thermal stress distribution of a trapezoidal TEC. Additionally, most studies assume a constant hot side and cold side temperature and ignore the effects of real working conditions—where the cold end has a thermal load and the hot end is connected to an advanced heat dissipation device—on the performance and reliability of TECs. The thermal load will cause higher local thermal stress, affecting the reliability of the device significantly.

Therefore, in this work, a full-scale 3D trapezoidal TEC model is constructed to study its cooling performance and mechanical reliability via the finite element simulation firstly. A power chip is fixed on the cold end of the trapezoidal TEC with thermal grease, and the advanced heat dissipation device connected to the hot end is simplified by the equivalent heat transfer coefficient, which is closer to the real working environment. Temperature-dependent characteristics of thermoelectric materials are considered. Subsequently, the effects of the input electrical current, thermoelectric leg height and the ratio of the area of the cold end of the thermoelectric leg to the area of its hot end on the cooling performance and thermal stress of the trapezoidal TEC are analyzed. These results in the article give us a better understanding of the cooling performance and reliability of the trapezoidal-shaped leg, which helps us to design the actual trapezoidal TEC.

2. Modelling

2.1. Physical Model

The schematic diagram of a trapezoidal TEC with variable cross-sectional area and a power chip is attached to its cold end through thermal grease is shown in Figure 1. The geometry dimensions of the TEC selected in this work are based on common commercial applications. The trapezoidal TEC

(30 × 30 mm) is made up of 142 thermoelectric legs. All leg dimensions are equal. The schematic of a thermoelectric pair in a rectangular TEC or a trapezoidal TEC is shown in Figure 2. The volume of the trapezoidal-shaped legs with different cross-sectional ratios remains constant, which is equal to that of the rectangular-shaped legs used in the conventional TEC. The geometric parameters of the rectangular TEC are used as the basic parameters in this study. These basic geometric parameters are listed in Table 1. The materials used in this work have been carefully selected considering their physical properties for optimal performance. The choice of thermoelectric materials directly affects the performance of TECs. Bismuth telluride (Bi_2Te_3) was selected as the thermoelectric material because it has the best thermoelectric properties at low temperature ranges. As a commercial material, it is widely used in thermoelectric coolers. Al_2O_3 was chosen as the substrate layer material for heat conduction and electrical insulation. Copper slices were used as conductive layers which connect the thermoelectric legs. The Sn-Pb solder was used as a welding layer in this study. Ceramic materials and thermoelectric materials are considered as brittle materials. Copper slices and solders were identified as elastoplastic materials for reducing thermal stress in the trapezoidal TEC [39]. The temperature dependent properties of thermoelectric leg materials used in this simulation are shown in Figure 3 and residual material properties are shown in Table 2.

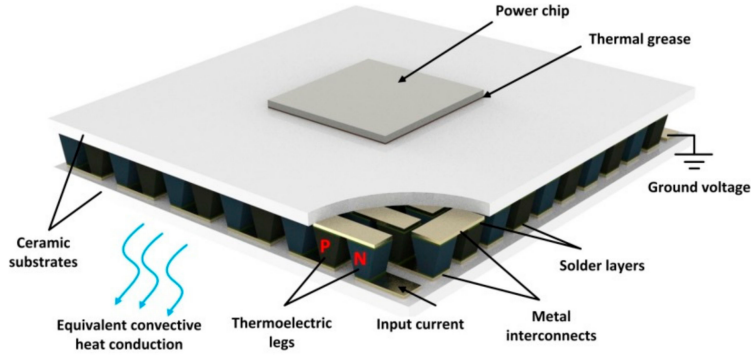

Figure 1. Schematic diagram of a trapezoidal thermoelectric coolers (TEC) with power chip system.

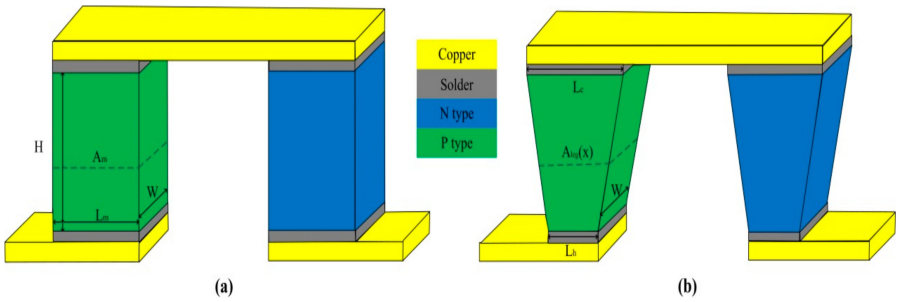

Figure 2. Geometric model of a thermoelectric pair: (**a**) rectangular TEC or (**b**) trapezoidal TEC.

Table 1. Basic geometric parameters of the rectangular TEC.

Parameter	Value
Leg height (mm)	1.6
Electrode thickness (mm)	0.2
Solder thickness (mm)	0.1
Substrate thickness (mm)	0.8
Cross-section area of the legs (mm^2)	1.4 × 1.4
pitch (mm)	1.0
Power chip thickness (mm)	0.4
Thermal grease thickness (mm)	0.1
Cross-section area of power chip (mm^2)	10 × 10

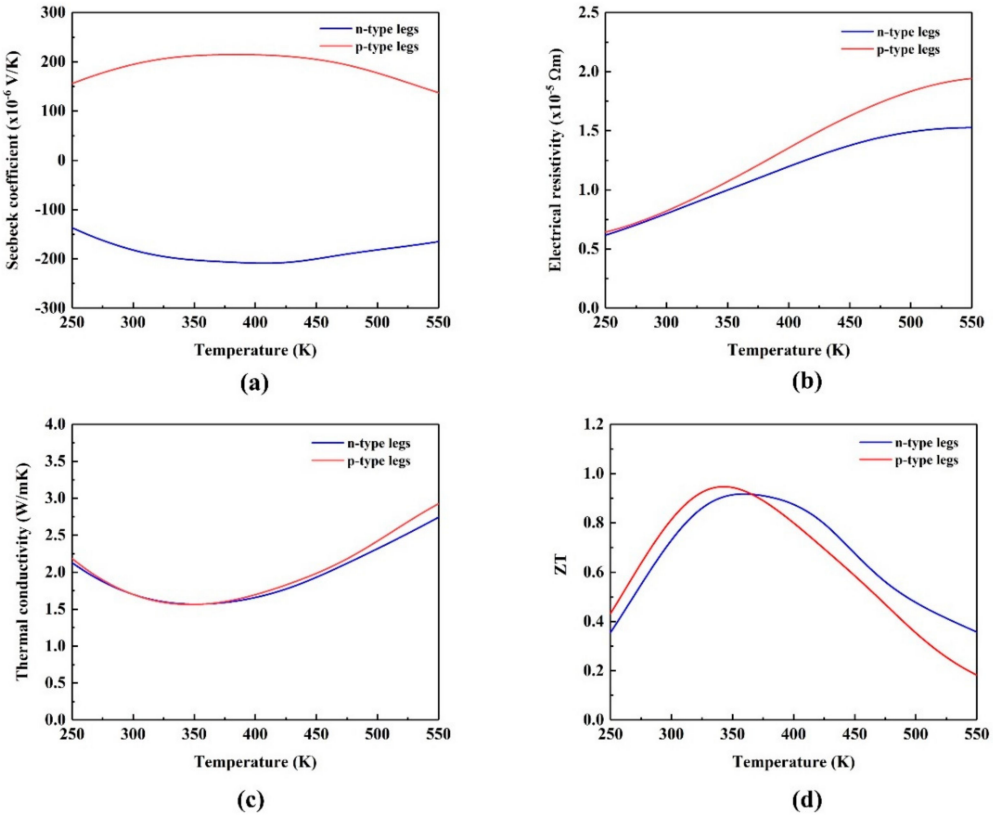

Figure 3. Temperature dependent thermoelectric material properties (**a**) Seebeck coefficient (**b**) electrical resistivity (**c**) thermal conductivity and (**d**) figure of merit (ZT) [40].

2.2. Thermo-Physical Properties

Figure 3 shows the temperature dependence of Bi_2Te_3 materials. Because of its bipolar diffusion effect, the Seebeck coefficient peaks around 400 K, and the thermal conductivity starts to rise at 350 K, making the extreme value of ZT appear at around 350 K. The electrical resistivity increases monotonously with temperature.

In the design of thermoelectric coolers, the electrical resistance causes Joule heat, the temperature inside the thermoelectric leg decreases as the electrical resistivity decreases, and the electrical resistivity determines the maximum current of the device. Thermal conductivity determines the maximum temperature difference of the device, lower thermal conductivity provides better cooling performance for thermoelectric coolers. The Seebeck coefficient is the most important parameter in the thermoelectric cooler, it directly determines the performance of the thermoelectric cooler. The maximum efficiency of a thermoelectric cooler is a function of the ZT, $ZT = S^2\sigma T/\kappa$. The ZT is proportional to the square of the Seebeck coefficient (S) and electrical conductivity (σ). It is inversely proportional to the thermal conductivity (κ). The ZT can effectively reflect the cooling performance of thermoelectric coolers.

Table 2. Other material properties used in this simulation [38,41].

Material	Thermal Conductivity (W/(m·K))	Electrical Conductivity (S/m)	Seebeck Coefficient (V/K)	Density (kg/m^3)	Specific Heat Capacity (J/kg·K)	Young's Modulus (GPa)	Coefficient of Thermal Expansion (1/K)	Poisson's Ratio
Ceramic	25	1×10^{-12}	0	3970	800	380	6.5×10^{-6}	0.22
Copper	385	5.9×10^{7}	6.5×10^{-6}	8930	386	115	1.7×10^{-5}	0.31
Solder	55	2×10^{7}	0	7240	210	44.5	2.7×10^{-5}	0.33
P-Bi_2Te_3	-	-	-	7740	154.4	65~59	0.8×10^{-5}~1.32×10^{-5}	0.23
N-Bi_2Te_3	-	-	-	7740	154.4	65~59	0.8×10^{-5}~1.32×10^{-5}	0.23
Power chip	420	1×10^{-14}	0	3100	800	410	4×10^{-6}	0.14
Thermal grease	1	2.5×10^{-12}	0	1630	1450	60	1.8×10^{-5}	0.19

2.3. Mathematical Model

The algebraic expressions on the variable cross-sectional area of the leg for the trapezoidal TEC, as expressed in Figure 2, and can be written as [42,43]:

$$A_{leg}(x) = \frac{A_c - A_h}{H}x + A_h, \tag{1}$$

where A_h is the cross-sectional area of hot end for thermoelectric legs, A_c is the cross-sectional area of cold end. H is the leg height. The ratio of the area of the cold end for the thermoelectric leg to the area of its hot end is defined as $R_A = A_c/A_h$.

The equation of the cross-sectional area of thermoelectric legs is rewritten:

$$A_{leg}(x) = A_m\left[1 + 2\frac{R_A - 1}{R_A + 1}\left(\frac{x}{H} - \frac{1}{2}\right)\right], \tag{2}$$

where A_m is the uniform (mid-height) cross-sectional area of the thermoelectric pin.

The total volume of each thermoelectric pin for the trapezoidal TEC can be calculated as:

$$V_{leg} = \frac{L_c + L_h}{2} \times W \times H = \frac{A_c + A_h}{2} \times H = L_m \times W \times H = A_m \times H, \tag{3}$$

where L_c and L_h are the leg length of the cold end and hot end of the trapezoidal TEC, respectively. L_m is the leg length for the rectangular TEC. W is the leg width.

The Fourier heat conduction rate along the x-axis is expressed as:

$$\dot{Q} = -kA_{leg}(x)\frac{dT}{dx}, \tag{4}$$

After substituting Equation (2) into Equation (4) and performing an integral operation, the Equation (4) is rewritten as:

$$\dot{Q} = \frac{2k\frac{A_m}{H}\left(\frac{R_A-1}{R_A+1}\right)}{In(R_A)}(T_h - T_c), \tag{5}$$

The overall thermal conductance of each thermoelectric leg pair is expressed as:

$$K = 2(k_p + k_n)\frac{\frac{A_m}{H}\left(\frac{R_A-1}{R_A+1}\right)}{In(R_A)}, \tag{6}$$

where k_p and k_n are the thermal conductivity for each p-type leg and n-type leg, respectively.

The total electrical resistance for each thermoelectric column pair is given as:

$$R = \left(\frac{1}{\sigma_p} + \frac{1}{\sigma_n}\right)\frac{1}{2\frac{A_m}{H}\left(\frac{R_A-1}{R_A+1}\right)}In(R_A), \tag{7}$$

where σ_p and σ_n are the electrical conductivity for each p-type leg and n-type leg, respectively.

2.4. Numerical Model

The numerical analysis for the trapezoidal TEC is segmented into the following two aspects: the thermoelectric analysis and thermal stress analysis. All thermoelectric effects are considered in both analytical models. The thermal stress distribution of the trapezoidal TEC is obtained by applying the temperature field value calculated from the thermoelectric analysis.

2.4.1. Mathematical Equations of Thermoelectric Analysis

Under the steady-state study, the three-dimensional heat flow equation and charge continuity equation of the trapezoidal TEC are described as Equations (8) and (9) [44]:

$$\nabla \cdot \vec{q} = Q, \tag{8}$$

$$\nabla \cdot \vec{J} = 0, \tag{9}$$

where $\vec{q}$, Q, $\vec{J}$, are the heat flux vector, Joule heating and electric current intensity vector, respectively.

The electric field $\vec{E}$, expressed by the electric scalar potential ϕ, is written in Equation (10):

$$\vec{E} = -\nabla\phi, \tag{10}$$

The matrix form of the thermoelectric constitutive equation is:

$$\vec{q} = [\pi] \cdot \vec{J} - [K] \cdot \nabla\vec{T}, \tag{11}$$

$$\vec{J} = [\sigma] \cdot \vec{E} - [\sigma] \cdot [S] \cdot \nabla\vec{T}, \tag{12}$$

where $[\pi]$, $[K]$, $[\sigma]$, $[S]$ are the Peltier coefficient matrix, thermal conductivity matrix, electric conductivity matrix and Seebeck coefficient matrix, respectively.

Substituting Equations (11) and (12) into Equations (8) and (9) can be written as:

$$\nabla \cdot [\pi] \cdot \vec{J} - \nabla \cdot [K] \cdot \nabla\vec{T} = Q, \tag{13}$$

$$\nabla \cdot [\sigma] \cdot \nabla\phi + \nabla \cdot [\sigma] \cdot [S] \cdot \nabla\vec{T} = 0, \tag{14}$$

2.4.2. Mathematical Equations of Thermal Stress Analysis

The thermal stress governing equation described by the displacement-strain equilibrium relationship is expressed as [45]:

$$\overline{\varepsilon}_{xx} = \frac{\partial\overline{u}}{\partial\overline{x}}, \ \overline{\varepsilon}_{yy} = \frac{\partial\overline{v}}{\partial\overline{y}}, \ \overline{\varepsilon}_{zz} = \frac{\partial\overline{w}}{\partial\overline{z}}, \tag{15}$$

$$\overline{\varepsilon}_{xy} = \frac{1}{2}\left(\frac{\partial\overline{u}}{\partial\overline{y}} + \frac{\partial\overline{v}}{\partial\overline{x}}\right), \ \overline{\varepsilon}_{yz} = \frac{1}{2}\left(\frac{\partial\overline{w}}{\partial\overline{y}} + \frac{\partial\overline{v}}{\partial\overline{z}}\right), \ \overline{\varepsilon}_{xz} = \frac{1}{2}\left(\frac{\partial\overline{w}}{\partial\overline{x}} + \frac{\partial\overline{u}}{\partial\overline{z}}\right), \tag{16}$$

An asymmetric Jacobian matrix is used to describe the dimensionless strain relation, as shown below:

$$\begin{bmatrix} \overline{\sigma}_{xx} \\ \overline{\sigma}_{yy} \\ \overline{\sigma}_{zz} \\ \overline{\sigma}_{yz} \\ \overline{\sigma}_{zx} \\ \overline{\sigma}_{xy} \end{bmatrix} = \frac{\overline{E}}{(1+v)(1-2v)} \begin{bmatrix} 1-v & v & v & 0 & 0 & 0 \\ v & 1-v & v & 0 & 0 & 0 \\ v & v & 1-v & 0 & 0 & 0 \\ 0 & 0 & 0 & 1-2v & 0 & 0 \\ 0 & 0 & 0 & 0 & 1-2v & 0 \\ 0 & 0 & 0 & 0 & 0 & 0 \end{bmatrix} \times \begin{Bmatrix} \overline{\varepsilon}_{xx} \\ \overline{\varepsilon}_{yy} \\ \overline{\varepsilon}_{zz} \\ \overline{\varepsilon}_{yz} \\ \overline{\varepsilon}_{zx} \\ \overline{\varepsilon}_{xy} \end{Bmatrix} - \begin{Bmatrix} 1 \\ 1 \\ 1 \\ 0 \\ 0 \\ 0 \end{Bmatrix} \frac{\overline{\alpha}\overline{E}\overline{T}}{1-2v} \tag{17}$$

The von Mises stress is used to express the value of thermal stress in this study. The three principal stress components are expressed as σ_1, σ_2 and σ_3, respectively. According to the shape change specific energy theory, the von Mises stress can be described by these three principal stresses as:

$$\sigma_{von} = \sqrt{\frac{(\sigma_1 - \sigma_2)^2 + (\sigma_2 - \sigma_3)^2 + (\sigma_3 - \sigma_1)^2}{2}}, \tag{18}$$

2.4.3. Boundary Conditions

These assumptions—that do not deviate significantly from reality—are introduced to simplify this simulation model. These simplified factors have negligible influence on the results:

- Steady state conditions are assumed in this study;
- Apart from the cold side and hot side for the trapezoidal TEC, all lateral surfaces are considered to be adiabatic;
- Electrical and thermal contact resistance are neglected;
- The thermal power of the power chip on the cold side of trapezoidal TEC is set to 5 W;
- The heat sink connected to the hot end of the trapezoidal TEC is assumed to be the equivalent convection heat transfer coefficient, its value is set to 1000 W/(m^2 K) to meet the range of forced convection heat conduction for water;
- The cold side and hot side of the trapezoidal TEC are fixed by clamps during thermal stress analysis.

2.4.4. Model Validation

The numerical results in this study were calculated by COMSOL Multiphysics 5.4 software. The cooling performance and thermal stress distribution for the trapezoidal TEC was obtained by the finite element method. The electrical currents, heat transfer in solids and solid mechanics interfaces were applied in this numerical simulation. To demonstrate the grid independence, three different mesh elements of 171040, 209655 and 266264 were investigated, as listed in Table 3. It can be seen that the values of the chip temperature, calculated by the three grid elements are basically same. The maximum deviation of the calculation result is less than 1% in the three grid systems. Therefore, the independence of the grid is confirmed. To decrease the computational cost, the mesh number of 171040 was chosen for the simulation analysis. In addition, in order to prove the correctness of the trapezoidal TEC simulation model, we compared the simulation results with the experimental results of Siddique et al. [17] and Erturun et al. [33], as shown in Figure 4a,b. The simulation environment and parameters were reset to be consistent with the experimental condition and parameters in the reference articles. It can be seen from both figures that the numerical results are consistent with the experimental results within the allowable error range. The deviation between the numerical and experimental results for power output is 4.87% and for height difference is 4.98%. Hence, the simulation model used in this article is accurate.

Table 3. Chip temperature under three grid systems.

Grid Number	Chip Temperature for I = 2 A (K)	Chip Temperature for I = 3 A (K)	Chip Temperature for I = 4 A (K)	Chip Temperature for I = 5 A (K)
171040	332.183	322.049	318.728	321.935
209655	332.224	322.091	318.762	321.961
266264	332.215	322.081	318.752	321.950

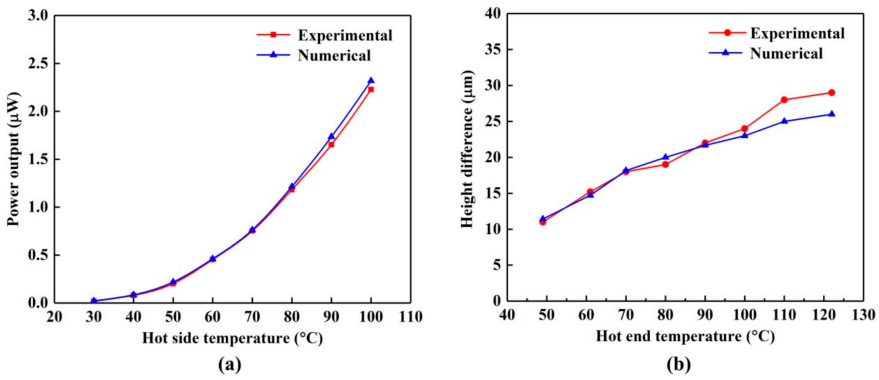

Figure 4. Comparison of simulation results and experimental results (**a**) performance validation and (**b**) thermal stress validation.

3. Results and Discussion

In order to keep the temperature of the chip below the critical temperature, the electrical current will be constantly changed when the trapezoidal TEC is functioning. Therefore, the performance and thermal stress distribution of trapezoidal TECs are affected by the electrical current. Besides, the performance and thermal stress distribution of trapezoidal TECs are also affected by the geometric parameters of the thermoelectric legs. The effects of the electrical current, the ratio of the area of the cold end of the thermoelectric leg to the area of its hot end, and leg height on the cooling performance and thermal stress distribution of trapezoidal TECs are analyzed in this section. The cross-sectional areas of the cold side and hot side for the thermoelectric legs corresponding to different R_A values are shown in Table 4.

Table 4. Various cross-sectional area ratio of the cold side to the hot side.

R_A	0.27	0.4	0.56	0.75	1	1.33	1.8	2.5	3.67
A_c (mm^2)	0.84	1.12	1.4	1.68	1.96	2.24	2.52	2.8	3.08
A_h (mm^2)	3.08	2.8	2.52	2.24	1.96	1.68	1.4	1.12	0.84

3.1. Influence of Electrical Current

The effect of the electrical current on the power chip temperature under different leg heights and ratios of the area of the cold end of the thermoelectric leg to the area of its hot end, is presented in Figure 5. It can be seen from Figure 5a,b, that the chip temperature first decreases and then increases with increasing electrical current. Before the electrical current reaches a critical value, the Peltier effect is dominant relative to the Joule heating effect. Therefore, the performance of the trapezoidal TEC is enhanced with the increase in the electrical current, making the chip temperature gradually decrease. On the contrary, when the electrical current exceeds the critical value, the Joule heating effect dominates, weakening the trapezoidal TEC performance and increasing the chip temperature again. When the electrical current is in the range of 3.5 A to 4 A, the chip temperature reaches its minimum value. The electrical current corresponding to the minimum chip temperature is defined as the optimal electrical current in this study. Figure 5a shows the different optimal electrical currents for various leg heights, when the ratio of the area of the cold side to area of the hot side of the trapezoidal-shaped legs is constant (i.e., R_A = 2.5), and the optimal electrical current decreases along with increasing leg height owing to the higher electrical resistance in the trapezoidal TEC with increasing leg height. Furthermore, the optimal electrical current first increases and then decreases with increasing R_A for the leg height of the trapezoidal TEC at a value of 1.6 mm, as shown in Figure 5b, and the optimal electrical current reaches the maximum value when R_A = 1 (the traditional rectangular TEC). For any two R_A values that are reciprocal to each other, their corresponding optimal electrical currents are equal, because they have the same electrical resistance and thermal resistance. The optimal electrical current defined in this section is used in the remaining sections of this study.

3.2. Influence of Leg Height

Figure 6 shows the influence of the leg height on the minimum chip temperature for different R_A values. The minimum chip temperature has the same decreasing trend as increasing leg height under different R_A values. It can be found that a higher leg height reduces the minimum chip temperature, which suggests that higher leg height is beneficial to enhance the cooling performance of the trapezoidal TECs. For example, the minimum chip temperature decreased by 4.5% for R_A = 1.8 when the leg height increased from 0.6 mm to 2.0 mm. The minimum chip temperature reached the minimum value of 284.085 K when H = 2.0 mm and R_A = 1.8, as shown in Figure 6.

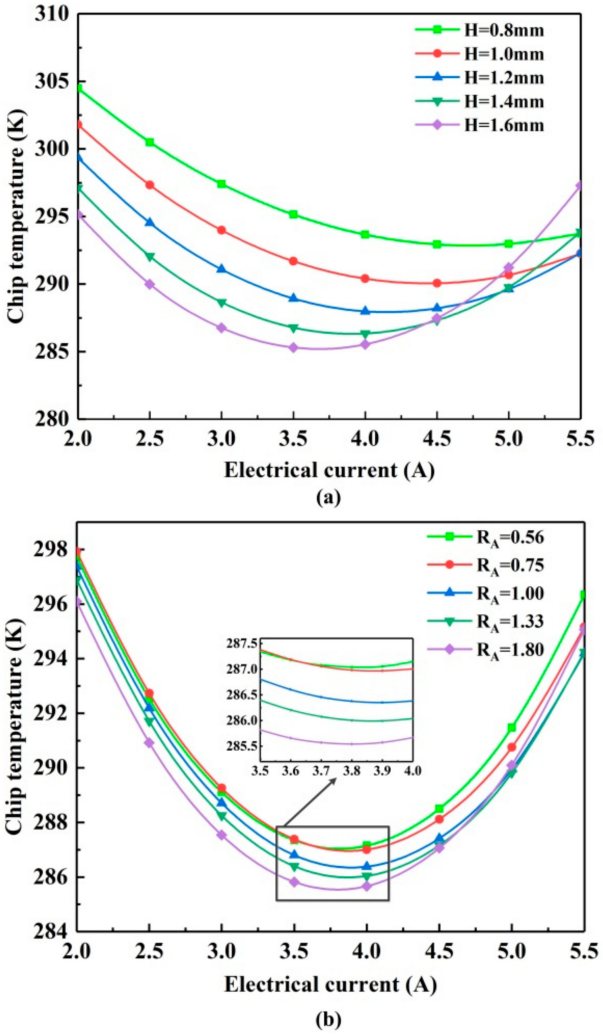

Figure 5. Variation of the chip temperature with the electrical current for (**a**) different leg heights when R_A = 2.5 and (**b**) different cross-sectional area ratios of the cold side to hot side for the legs when H = 1.6 mm.

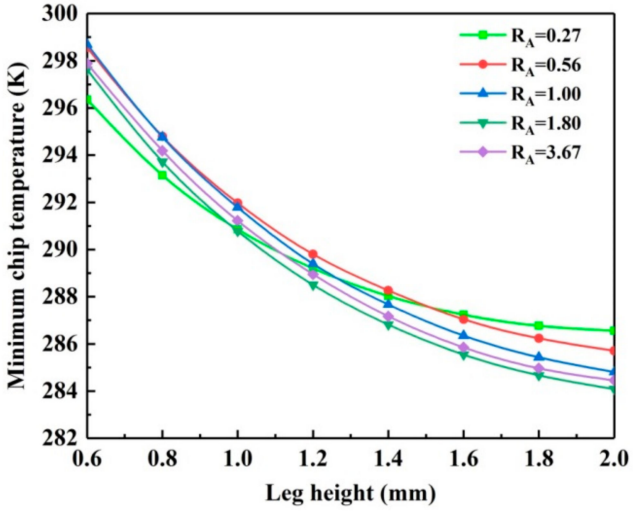

Figure 6. Variation of the minimum chip temperature with leg height for different R_A.

The main reason for this phenomenon is derived from the change of leg height leading to the change of all electrical resistances and thermal conductance for the trapezoidal TEC. From Equations (6) and (7), the overall thermal conductance of each thermoelectric leg pair is inversely proportional to the leg height, and the total electrical resistance of each thermoelectric leg pair is proportional to the leg height. The higher leg height leads to an increase in the electrical resistance of the leg and generates more Joule heat, causing a decrease in the thermal conductance of the leg and the Fourier heat transfer. Hence, a larger temperature difference is generated as increasing leg height between the hot side and cold side of the trapezoidal TEC, reduces the temperature of the chip.

3.3. Influence of Cross-Sectional Area Ratio

To illustrate the principle of variable cross-sectional area design, Figure 7 shows the spatial temperature distribution of the rectangular-shaped and trapezoidal-shaped leg for R_A = 1 and 2.5 when H = 1.6 mm. The temperature distribution of the trapezoidal-shaped leg along the leg height is different from that of the rectangular-shaped leg. As shown in Figure 3, the thermal conductivity, electrical resistivity, Seebeck coefficient and ZT for thermoelectric materials are all temperature-dependent. The variable cross-sectional area design can adjust the temperature distribution along the leg height compared with a constant cross-sectional area design. Therefore, compared with the rectangular-shaped thermoelectric leg, these thermo-physical properties of the material in the trapezoidal-shaped thermoelectric leg vary with the change in spatial temperature distribution, which affects the performance of the trapezoidal thermoelectric cooler.

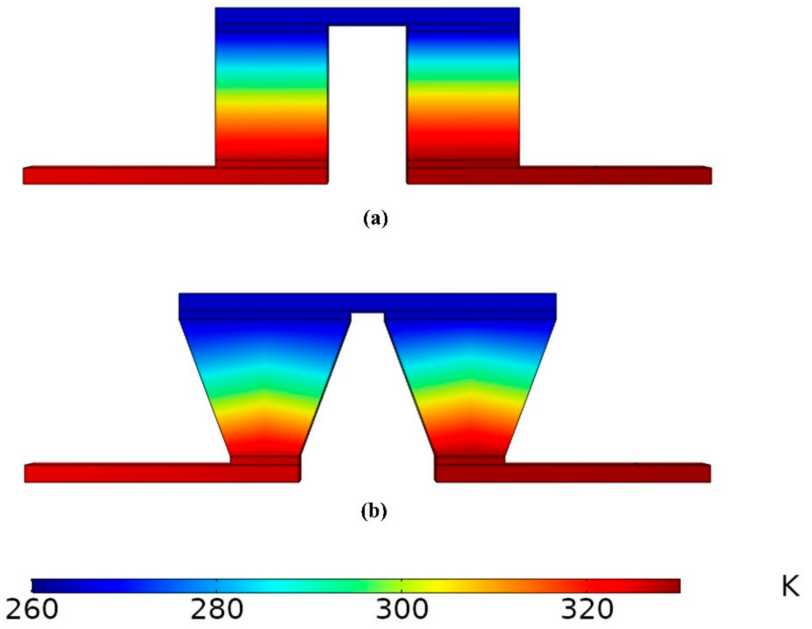

Figure 7. Temperature distributions of thermoelectric legs when H = 1.6 mm: (**a**) R_A = 1; (**b**) R_A = 2.5.

The influence of the ratio of the cross-sectional area of the cold side to that of the hot side of the thermoelectric leg on the minimum chip temperature at different leg heights is shown in Figure 8. The traditional rectangular TEC is expressed as R_A = 1. It can be seen that the variation tendency of the minimum chip temperature when H = 1.6 mm is different from the other leg heights, as is the increase in R_A. The minimum temperature of a chip cooled by a trapezoidal TEC is lower than the minimum temperature of a chip cooled by a rectangular TEC. For instance, the minimum chip temperature corresponding to the trapezoidal TEC is 1.2 K lower than the minimum chip temperature corresponding to the rectangular TEC when H = 1.6 mm. The minimum chip temperature decreases more significantly at $R_A > 1$ compared to $R_A < 1$. This indicates that the area of the cold side for the

trapezoidal TEC is larger than that of its hot side, which is more conducive to improving the cooling performance of the trapezoidal TEC. The minimum value of the minimum chip temperature always occurs at R_A = 2.5 in this figure.

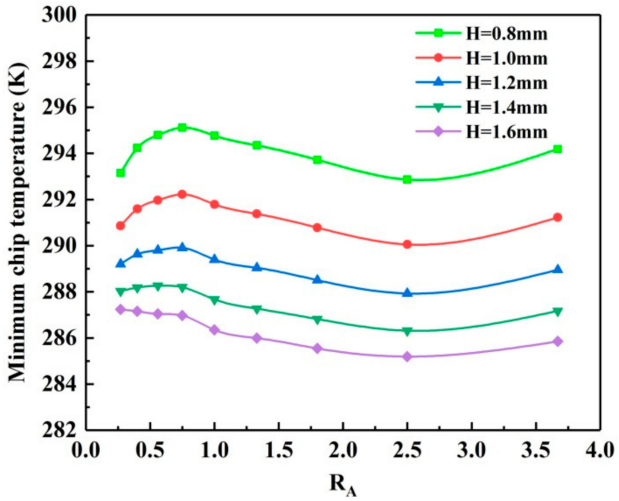

Figure 8. Variation of the minimum chip temperature with cross-sectional area ratios of the cold to hot ends of the legs for different H.

The variation tendency of the minimum chip temperature with increasing cross-sectional area ratio under different leg heights is mainly determined by the competitive relationship between the two effects. The trapezoidal-shaped leg changes the local electrical current density and local thermal resistance. They are no longer symmetrically distributed along the leg height. The electrical current density becomes larger at a smaller cross-sectional area, which generates more heat per unit volume. This phenomenon is called the Joule heating effect. Nevertheless, the smaller thermal resistance at the larger cross-sectional area causes more heat to be more easily transferred to the larger cross-sectional area end. This behavior is referred as the heat conduction effect. For example, when H = 1.2 mm, the minimum chip temperature increases first as the cross-sectional area ratio increases, indicating that increasing R_A makes the heat conduction effect dominate over the Joule heating effect at this stage. Afterwards, when R_A reaches a critical value, the Joule heating effect begins to dominate and the chip temperature begins to decrease. This occurs up until the point when R_A value is too large (R_A = 2.5), when the heat conduction effect once again dominates, making the minimum chip temperature rises again. When the leg height value is 1.6 mm, there is no first stage because the higher leg height weakens the heat conduction effect, a smaller cross-sectional area ratio is needed to make the heat conduction effect dominate.

From above results shown in Figures 6 and 8, the minimum chip temperature is determined by the leg height and the ratio of the area of the cold end of the thermoelectric leg to the area of its hot end. They are interdependent. It can be seen that the leg height has a more obvious effect on the minimum chip temperature than the cross-sectional area ratio, as shown in Figure 9. Compared to the original rectangular thermoelectric cooler, the minimum chip temperature is reduced by 0.87% under the trapezoidal thermoelectric cooler with optimized geometry.

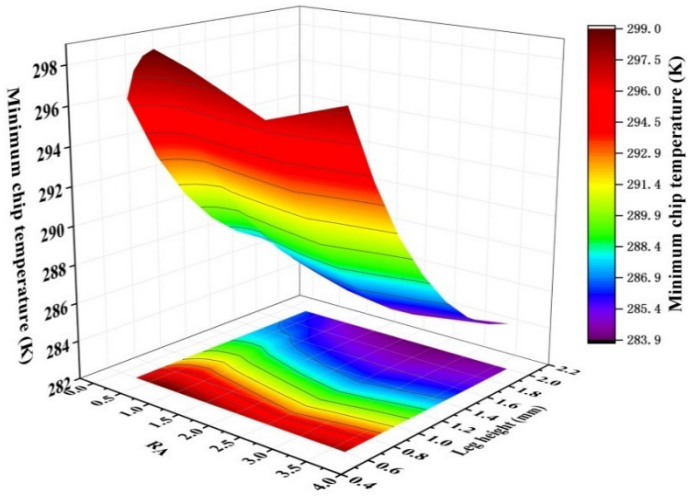

Figure 9. Variation of the minimum chip temperature with cross-sectional area ratios of the cold to hot ends of the legs and leg heights.

3.4. Thermal Stress Analysis

It is of importance to carry out a thermal stress analysis of trapezoidal TECs to increase its operating lifespan. The von Mises stress nephogram of a full-scale trapezoidal-shaped thermoelectric leg is shown in Figure 10 at H = 1.6 mm, I = 4 A. It can be found that the maximum von Mises stress appears on contact surfaces between the thermoelectric legs and solder layers. When $R_A < 1$, the maximum von Mises stress is generated on the cold side of the thermoelectric legs. When $R_A > 1$, the maximum von Mises stress is generated on the hot side of the thermoelectric legs. Furthermore, the maximum von Mises stress is generated at the edge of thermoelectric legs. These positions are easily destroyed first. From this figure, it can also be seen that the hot side and cold side of the trapezoidal-shaped thermoelectric legs generate a non-uniform thermal stress distribution, and the thermal stress for the thermoelectric legs at the edge of the chip is greater. This is due to the inhomogeneous temperature distribution resulting in a large local thermal stress gradient.

Figure 11 shows the influence of leg height on the maximum von Mises stress for the thermoelectric leg at different R_A. The maximum von Mises stress for the thermoelectric leg reduces as leg height is increased due to the decreasing temperature gradient, which indicates that the reliability of the trapezoidal TEC with a higher leg height is better. In addition, we observed that the maximum von Mises stress for the trapezoidal-shaped leg with variable cross-sectional area decreases more obviously as leg height increases, compared with the rectangular-shaped leg with a constant cross-sectional area. Taking $R_A = 1.8$ as an example, the maximum von Mises stress decreases by 46.7% as the leg height increases from 0.6 mm to 2.0 mm.

The influence of the ratio of the area of the cold end of the thermoelectric leg to the area of its hot end on the maximum von Mises stress of the thermoelectric leg is shown in Figure 12. As the R_A increases, the maximum von Mises stresses have the same changing trend at different leg heights. It can be seen that the maximum von Mises decreases first, then increases, and finally decreases as the R_A value increases. The minimum value for the maximum von Mises stress always occurs at $R_A = 1$, which indicates that the mechanical reliability of the rectangular-shaped leg with constant cross-sectional area compared with that of the trapezoidal-shaped leg with non-constant cross-sectional area is better. Meanwhile, when the R_A value exceeds 2.5, the maximum von Mises stress begins to decrease. From Figures 11 and 12, it can be seen that the minimum value for the maximum thermal stress of the thermoelectric leg is reached when H = 2 mm and $R_A = 1$. The maximum von Mises stress of the leg for the trapezoidal thermoelectric cooler with optimal cooling performance has increased by 40.1% compared to the original rectangular thermoelectric cooler.

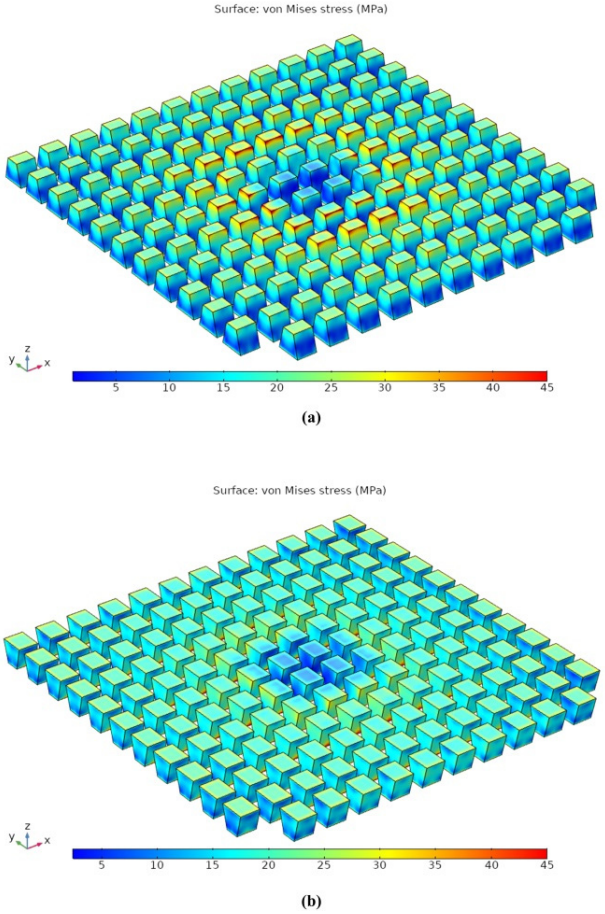

Figure 10. The von Mises stress nephogram of full-scale trapezoidal-shaped thermoelectric legs when H = 1.6 mm, I = 4 A (**a**) R_A = 0.56 and (**b**) R_A = 1.8.

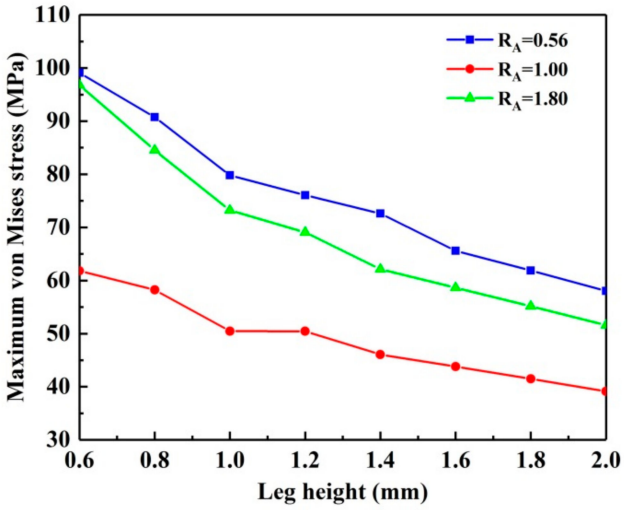

Figure 11. Change of the maximum von Mises stress with leg height for different R_A.

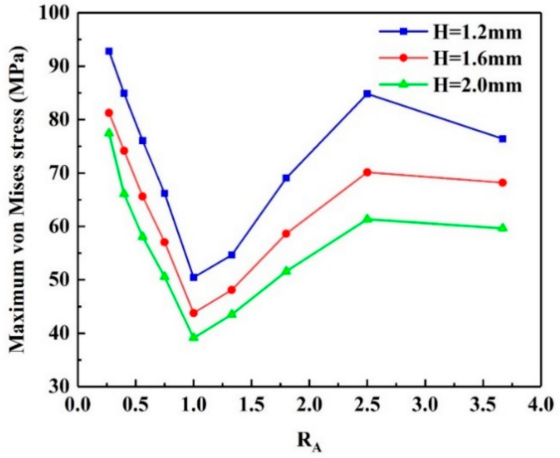

Figure 12. Change of the maximum von Mises stress with cross-sectional area ratio of the cold side to hot side of the leg for different H.

From the above analysis, it can be seen that a higher thermoelectric pin not only improves cooling performance but also enhances the mechanical reliability of the trapezoidal TEC. However, compared with the rectangular-shaped leg with a constant cross-sectional area, the trapezoidal-shaped leg with a variable cross-sectional area improves the performance while reducing the mechanical reliability of the trapezoidal TEC. Therefore, practical applications, the leg height and the ratio of the cross-sectional area of the cold end to that of the hot end for the trapezoidal-shaped thermoelectric leg should be carefully selected according to the actual needs, the cooling performance and mechanical reliability should be considered at the same time.

4. Conclusions

In summary, the cooling performance and mechanical reliability of a full-scale trapezoidal TEC with a non-constant cross-sectional area were studied via finite element analysis. The thermal boundary conditions were simulated in a similar manner to the actual experimental conditions. The effects of the input electrical current, leg height, and the ratio of the area of the cold end of the thermoelectric leg to the area of its hot end on the minimum chip temperature and the maximum thermal stress for the leg were analyzed in detail, and a comparison between trapezoidal TEC and rectangular TEC was carried out. The calculated thermal stress nephogram of the trapezoidal-shaped legs is used to better visualize the thermal stress distribution of the legs. Some important conclusions are as follows:

1. The optimal electrical current corresponding to the trapezoidal-shaped thermoelectric leg under different geometric parameters is different. The optimal electrical current should be used when analyzing the performance and thermal stress of the trapezoidal TEC.
2. Increasing the thermoelectric leg height simultaneously improves the cooling performance and mechanical reliability of the trapezoidal TEC. For R_A = 1.8, the minimum chip temperature decreased by 4.5% and the maximum von Mises stress of the leg decreased by 46.7% as the leg height increased from 0.6 mm to 2.0 mm.
3. Compared to the rectangular TEC, the variable cross-sectional design for the trapezoidal TEC improves the cooling performance. The minimum chip temperature was reduced by 0.87% under the trapezoidal thermoelectric cooler with optimized geometry.
4. The maximum von Mises stress for the trapezoidal-shaped leg was greater than that of the rectangular-shaped leg. The maximum von Mises stress of the leg for the trapezoidal thermoelectric cooler with optimal cooling performance increased by 40.1% compared to the original rectangular thermoelectric cooler. Therefore, both the cooling performance and reliability need to be considered at the same time when designing a trapezoidal TEC.

Author Contributions: Conceptualization, T.L.; methodology, T.L.; writing—original draft preparation, T.L.; writing—review and editing, P.N. (Pingfan Ning); visualization, J.Z.; supervision, Y.L. and P.N. (Pingjuan Niu); project administration, P.N. (Pingjuan Niu). All authors have read and agreed to the published version of the manuscript.

Funding: This research was funded by the Science and Technology Development Fund of Tianjin Education Commission for Higher Education (Grant No. 2018KJ210).

Conflicts of Interest: The authors declare no conflict of interest.

References

1. Cai, Y.; Wang, Y.; Liu, D.; Zhao, F.Y. Thermoelectric cooling technology applied in the field of electronic devices: Updated review on the parametric investigations and model developments. *Appl. Therm. Eng.* **2019**, *148*, 238–255. [CrossRef]
2. Sarafraz, M.M.; Pourmehran, O.; Yang, B.; Arjomandi, M. Assessment of the thermal performance of a thermosyphon heat pipe using zirconia-acetone nanofluids. *Renew. Energ.* **2019**, *136*, 884–895. [CrossRef]
3. Sarafraz, M.M.; Yang, B.; Pourmehran, O.; Arjomandi, M.; Ghomashchi, R. Fluid and heat transfer characteristics of aqueous graphene nanoplatelet (GNP) nanofluid in a microchannel. *Int. Commum. Heat Mass Transf.* **2019**, *107*, 24–33. [CrossRef]
4. Pan, M.Q.; Zhong, Y.J. Experimental and numerical investigation of a thermal management system for a Li-ion battery pack using cutting copper fiber sintered skeleton/paraffin composite phase change materials. *Int. J. Heat Mass Transf.* **2018**, *126*, 531–543. [CrossRef]
5. Pourmehran, O.; Sarafraz, M.M.; Rahimi-Gorji, M.; Ganji, D.D. Rheological behaviour of various metal-based nano-fluids between rotating discs: A new insight. *J. Taiwan Inst. Chem. E* **2018**, *88*, 37–48. [CrossRef]
6. Nazari, S.; Ellahi, R.; Sarafraz, M.M.; Safaei, M.R.; Asgari, A.; Akbari, O.A. Numerical study on mixed convection of a non-Newtonian nanofluid with porous media in a two lid-driven square cavity. *J. Therm. Anal. Calorim.* **2020**, *140*, 1121–1145. [CrossRef]
7. Sun, H.N.; Gil, S.U.; Liu, W.; Liu, Z.C. Structure optimization and exergy analysis of a two-stage TEC with two different connections. *Energy* **2019**, *180*, 175–191. [CrossRef]
8. Xu, G.L.; Duan, Y.; Chen, X.T.; Ming, T.Z.; Huang, X.M. Effects of thermal and electrical contact resistances on the performance of a multi-couple thermoelectric cooler with non-ideal heat dissipation. *Appl. Therm. Eng.* **2020**, *169*, 114933. [CrossRef]
9. Simon, J.; Guélou, G.; Srinivasan, B.; Berthebaud, D.; Mori, T.; Maignan, A. Exploring the thermoelectric behavior of spark plasma sintered $Fe_{7-x}Co_xS_8$ compounds. *J. Alloys Compd.* **2020**, *819*, 152999. [CrossRef]
10. Srinivasan, B.; Berthebaud, D.; Mori, T. Is LiI a Potential Dopant Candidate to Enhance the Thermoelectric Performance in Sb-Free GeTe Systems? A Prelusive Study. *Energies* **2020**, *13*, 643. [CrossRef]
11. Kishore, R.A.; Kumar, P.; Sanghadasa, M.; Priya, S. Taguchi optimization of bismuth-telluride based thermoelectric cooler. *J. Appl. Phys.* **2017**, *122*, 025109. [CrossRef]
12. Zhu, W.; Deng, Y.; Wang, Y.; Wang, A.L. Finite element analysis of miniature thermoelectric coolers with high cooling performance and short response time. *Microelectron. J.* **2013**, *44*, 860–868. [CrossRef]
13. Huang, Y.X.; Wang, X.D.; Cheng, C.H.; Lin, D.T.W. Geometry optimization of thermoelectric coolers using simplified conjugate-gradient method. *Energy* **2013**, *59*, 689–697. [CrossRef]
14. Abid, M.; Somdalen, R.; Rodrigo, M.S. Design Optimization of a Thermoelectric Cooling Module Using Finite Element Simulations. *J. Electron. Mater.* **2018**, *47*, 4845–4854. [CrossRef]
15. Gong, T.R.; Gao, L.; Wu, Y.J.; Zhang, L.; Yin, S.; Li, J.T.; Ming, T.Z. Numerical simulation on a compact thermoelectric cooler for the optimization design. *Appl. Therm. Eng.* **2019**, *146*, 815–825. [CrossRef]
16. Thimont, Y.; LeBlanc, S. The impact of thermoelectric leg geometries on thermal resistance and power output. *J. Appl. Phys.* **2019**, *126*, 095101. [CrossRef]
17. Siddique, A.M.; Mahmud, S.; Van Heyst, B. Performance comparison between rectangular and trapezoidal-shaped thermoelectric legs manufactured by a dispenser printing technique. *Energy* **2020**, *196*, 117089. [CrossRef]
18. Su, N.; Zhu, P.F.; Pan, Y.H.; Li, F.; Li, B. 3D-printing of shape-controllable thermoelectric devices with enhanced output performance. *Energy* **2020**, *195*, 116892. [CrossRef]

19. Siddique, A.M.; Venkateshwar, K.; Mahmud, S.; Van Heyst, B. Performance analysis of bismuth-antimony-telluride-selenium alloy-based trapezoidal-shaped thermoelectric pallet for a cooling application. *Energy Convers. Manag.* **2020**, *222*, 113245. [CrossRef]
20. Lamba, R.; Kaushik, S.C. Thermodynamic analysis of thermoelectric generator including influence of Thomson effect and leg geometry configuration. *Energy Convers. Manag.* **2017**, *144*, 388–398. [CrossRef]
21. Wang, R.C.; Meng, Z.H.; Luo, D.; Yu, W.; Zhou, W.Q. A Comprehensive Study on X-Type Thermoelectric Generator Modules. *J. Electron. Mater.* **2020**, *49*, 4343–4354. [CrossRef]
22. Trung, N.H.; Toan, N.V.; Ono, T. Flexible thermoelectric power generator with Y-type structure using electrochemical deposition process. *Appl. Energy* **2018**, *210*, 467–476.
23. Lin, S.M.; Yu, J.L. Optimization of a trapezoid-type two-stage Peltier couples for thermoelectric cooling applications. *Int. J. Refrig.* **2016**, *65*, 103–110. [CrossRef]
24. Lv, H.; Wang, X.D.; Wang, T.H.; Cheng, C.H. Improvement of transient supercooling of thermoelectric coolers through variable semiconductor cross-section. *Appl. Energy* **2016**, *164*, 501–508. [CrossRef]
25. Gao, Y.W.; Meng, J.H.; Liu, H.B.; Chen, W.H.; Wang, X.D. Transient supercooling behaviors of a novel two-stage Peltier cooler. *Appl. Therm. Eng.* **2018**, *143*, 248–256. [CrossRef]
26. Qiu, C.S.; Shi, W.K. Comprehensive modeling for optimized design of a thermoelectric cooler with non-constant cross-section: Theoretical considerations. *Appl. Therm. Eng.* **2020**, *176*, 115384. [CrossRef]
27. Lamba, R.; Maikandan, S.; Kaushik, S.C.; Tyagi, S.K. Thermodynamic modelling and performance optimization of trapezoidal thermoelectric cooler using genetic algorithm. *Therm. Sci. Eng. Prog.* **2018**, *6*, 236–250. [CrossRef]
28. Cui, Y.J.; Wang, B.L.; Wang, K.F. Thermally induced vibration and strength failure analysis of thermoelectric generators. *Appl. Therm. Eng.* **2019**, *160*, 113991. [CrossRef]
29. Karri, N.K.; Mo, C. Reliable Thermoelectric Module Design under Opposing Requirements from Structural and Thermoelectric Considerations. *J. Electron. Mater.* **2018**, *47*, 3127–3135. [CrossRef]
30. Wu, Y.J.; Ming, T.Z.; Li, X.H.; Pan, T.; Peng, K.Y.; Luo, X.B. Numerical simulations on the temperature gradient and thermal stress of a thermoelectric power generator. *Energy Convers. Manag.* **2014**, *88*, 915–927. [CrossRef]
31. Jia, X.D.; Gao, Y.W. Estimation of thermoelectric and mechanical performances of segmented thermoelectric generators under optimal operating conditions. *Appl. Therm. Eng.* **2014**, *73*, 335–342. [CrossRef]
32. Al-Merbati, A.S.; Yilbas, B.S.; Sahin, A.Z. Thermodynamics and thermal stress analysis of thermoelectric power generator: Influence of pin geometry on device performance. *Appl. Therm. Eng.* **2013**, *50*, 683–692. [CrossRef]
33. Erturun, U.; Erermis, K.; Mossi, K. Effect of various leg geometries on thermo-mechanical and power generation performance of thermoelectric devices. *Appl. Therm. Eng.* **2014**, *73*, 128–141. [CrossRef]
34. Yilbas, B.S.; Akhtar, S.S.; Sahin, A.Z. Thermal and stress analyses in thermoelectric generator with tapered and rectangular pin configurations. *Energy* **2016**, *114*, 52–63. [CrossRef]
35. Ibeagwu, O.I. Modelling and comprehensive analysis of TEGs with diverse variable leg geometry. *Energy* **2019**, *180*, 90–106. [CrossRef]
36. Wang, W.C.; Chang, Y.L. Experimental Investigation of Thermal Deformation in Thermoelectric Coolers. *Strain* **2011**, *47*, 232–237. [CrossRef]
37. Gong, T.R.; Wu, Y.J.; Gao, L.; Zhang, L.; Li, J.T.; Ming, T.Z. Thermo-mechanical analysis on a compact thermoelectric cooler. *Energy* **2019**, *172*, 1211–1224. [CrossRef]
38. Gong, T.R.; Gao, L.; Wu, Y.J.; Tan, H.S.; Qin, F.; Ming, T.Z.; Li, J.T. Transient thermal stress analysis of a thermoelectric cooler under pulsed thermal loading. *Appl. Therm. Eng.* **2019**, *162*, 114240. [CrossRef]
39. Shittu, S.; Li, G.Q.; Xuan, Q.D.; Zhao, X.D.; Ma, X.L.; Cui, Y. Electrical and mechanical analysis of a segmented solar thermoelectric generator under non-uniform heat flux. *Energy* **2020**, *199*, 117433. [CrossRef]
40. Shen, Z.G.; Liu, X.; Chen, S.; Wu, S.Y.; Xiao, L.; Chen, Z.X. Theoretical analysis on a segmented annular thermoelectric generator. *Energy* **2018**, *157*, 297–313. [CrossRef]
41. Shittu, S.; Li, G.Q.; Zhao, X.D.; Ma, X.L.; Akhlaghi, Y.G.; Ayodele, E. High performance and thermal stress analysis of a segmented annular thermoelectric generator. *Energy Convers. Manag.* **2019**, *184*, 180–193. [CrossRef]
42. Liu, H.B.; Meng, J.H.; Wang, X.D.; Chen, W.H. A new design of solar thermoelectric generator with combination of segmented materials and asymmetrical legs. *Energy Convers. Manag.* **2018**, *175*, 11–20. [CrossRef]

43. Sahin, A.Z.; Yilbas, B.S. The thermoelement as thermoelectric power generator: Effect of leg geometry on the efficiency and power generation. *Energy Convers. Manag.* **2013**, *65*, 26–32. [CrossRef]
44. Shen, L.M.; Zhang, W.S.; Liu, G.Y.; Lu, Q.Q.; Chen, H.X.; Huang, Q.J. Performance enhancement investigation of thermoelectric cooler with segmented configuration. *Appl. Therm. Eng.* **2020**, *168*, 114852. [CrossRef]
45. Yu, J.; Kong, L.; Zhu, Q.S.; Zhu, H.J.; Wang, H.Q.; Guan, J.L.; Yan, Q. Thermal Stress Analysis of a Segmented Thermoelectric Generator under a Pulsed Heat Source. *J. Electron. Mater.* **2020**, *49*, 4392–4402. [CrossRef]